Programmable 3-D surfaces using origami tessellations

Hang Yuan, James Pikul, Cynthia Sung

Abstract: *We present an origami-inspired approach to reconfigurable surfaces. A circular origami tessellation with the ability to extend and flatten was designed to approximate radially symmetric 3-D surfaces. The pattern exhibits snap-through effects, allowing desired 3-D shapes to be maintained indefinitely without additional infrastructure or energy input. We characterize the geometry of the fold pattern and its resulting 3-D shape, present a strategy for reconfiguration, and demonstrate this strategy for surfaces with positive, negative, and zero Gaussian curvature.*

1 Introduction

Origami-inspired engineering has enabled new designs and functionality by leveraging 2-D sheets that transform into 3-D shapes using folds [Peraza-Hernandez et al. 14]. This 2-D to 3-D transformation allows complex structures to be formed out of uniform materials using fast, inexpensive fabrication and assembly methods. As a result, folding has been used for rapid prototyping and manufacturing in applications as diverse as packaging [Dai and Cannella 08], medicine [Edmondson et al. 13], emergency relief [Thrall and Quaglia 14], and robotics [Rus and Sung 18; Hoover et al. 08].

In this work, we are interested in how origami can be used to create programmable surfaces. Previous results in origami design have shown that arbitrary shapes can be folded from a single sheet [Demaine and Tachi 17]. Universal fold patterns even exist that can fold and refold into arbitrary 3-D shapes within a given resolution [Benbernou et al. 11; Hawkes et al. 10]. However, for these reconfigurable designs, each individual fold must be actuated over the course of a complex folding sequence, making control and actuation complicated.

Low degree of freedom deployment can be achieved by including kinematic constraints in a fold pattern. For example, many origami tessellations have only a few degrees of freedom [Overvelde et al. 16; Evans et al. 15; Filipov et al. 15] and can be folded or unfolded with one actuator. These designs can be modified to

approximate curved surfaces through local changes in the fold pattern [Dudte et al. 16]. The tradeoff is that because the 3-D surface is programmed into the fold pattern itself and because all units in the fold pattern are coupled, local deformations are not possible and the tessellation is not reconfigurable by default.

We present an origami design that maintains low degree of freedom transformation while enabling 3-D reconfiguration. The design is a radially symmetric structure that can reconfigure by selectively expanding or flattening entire rings to produce a desired height profile. Our results build upon our previous work in [Pikul et al. 17], where we were able to program the 3-D shape of inflated elastomer sheets by controlling radial strain with embedded non-woven fabrics. Unlike this previous work, which relied on an external pressure source, our origami pattern exhibits snap-through effects, allowing desired 3-D shapes to be maintained indefinitely without additional infrastructure or energy input.

The main contributions of this paper are:

- A radially symmetric origami tessellation with the ability to approximate curved surfaces;
- A parameterization of this pattern that provides guidelines for design;
- A procedure for converting a desired surface into a configuration for the structure; and
- Experimental validation of reconfiguration into five surfaces of different curvatures.

The remainder of this paper is organized as follows. Section 2 describes our approach to origami design. Section 3 describes and characterizes our final crease pattern. Section 4 details our reconfiguration strategy. Section 5 discusses our experimental results. Section 6 concludes with directions for future work.

2 Design Exploration

2.1 Early Attempts

Our goal is to create an origami pattern with the ability to reconfigure into multiple different 3-D surfaces with minimal actuation. To achieve this property, we started with various tessellation patterns that have been studied. Some of the examples are shown in Figure 1. Figure 1(a), (b), (c) are the origami flasher [Lang et al. 16], the origami square twist tessellation [Silverberg et al. 15], the origami washer [Liu et al. 17], respectively. All three of these models are globally expanding patterns.

To enable local expansion, we considered strategies to decouple the tessellation units. Figure 1(d) shows an example of a modification to the origami washer where the sectors of the pattern can move independently. The resulting model was able to expand and contract in the radial direction by collapsing sectors, but it was still not able to deform out-of-plane.

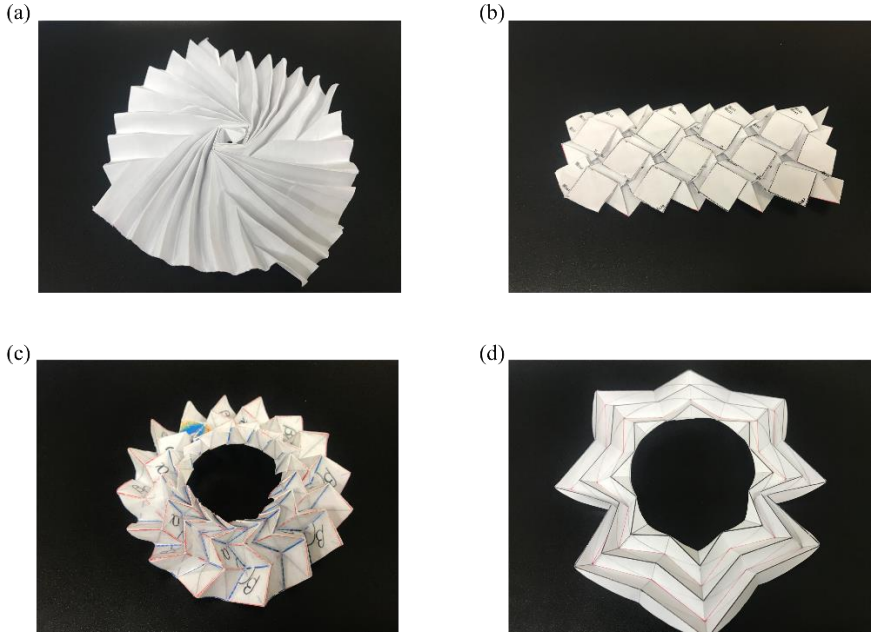

Figure 1: *Models of some early attempts. (a) origami flasher [Lang et al. 2016], (b) origami square twists [Silverberg et al. 2015], (c) origami washer [Liu et al. 2017], (d) modified origami washer.*

2.2 Folding from 3-D to 2-D

One of the main differences between origami-inspired design and other mechanical devices is that unlike general mechanisms, paper is not able to stretch. Tessellations and other expanding origami models address this issue by tucking material away in the shrunken state to allow for the additional material needed during expansion. Our main insight was that rather than folding a flat sheet, we should therefore start with a desired 3-D surface. We redirected our strategy to folding a cone into a flattened 2-D state.

We applied a similar strategy to the one used in Figure 1(d) to convert circumferential expansion to radial expansion by modifying the creases of a primal-dual tessellation [Lang 18]. We first glued the two ends of the modified pattern to make a cylinder. The resulting model was not completely flat, so we introduced additional folds by squashing the structure. By observing the new folds that were created by the squash and utilizing known relationships for flat foldability [Demaine and O'Rourke 08], we reconstructed the creases into the original fold pattern. Finally, we changed the dimension of different layers, to create rings of different radii.

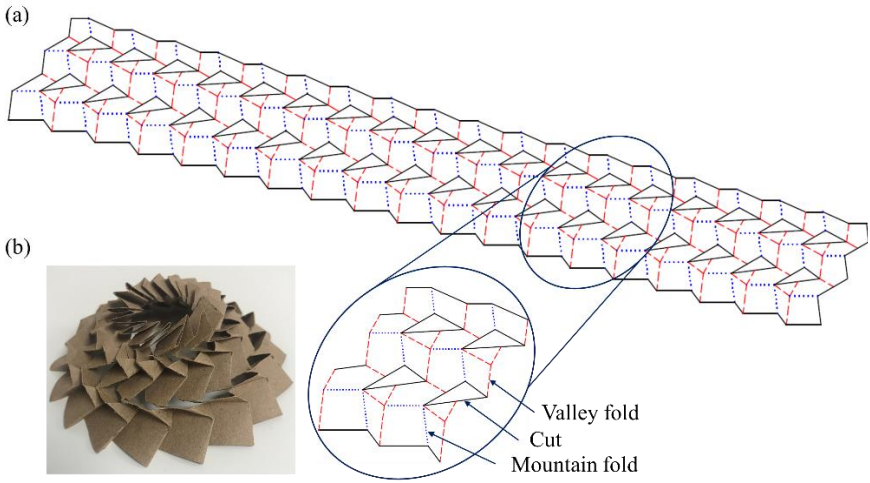

Figure 2: *First origami model modified based on the primal-dual tessellation [Lang 2018]. (a) crease pattern, dotted lines: mountain fold; dashed lines: valley fold; solid lines: cuts; (b) folded model.*

The result of this process was a collapsed cone with the ability to deform from flattened to fully extended state, but similarly to our previously explored tessellations, the motion of all the layers was coupled. We therefore tested two strategies for decoupling layer actuation to enable local deformations.

We first experimented with decoupling layers by adding cuts. Figure 2(a) shows one such trial pattern. Blue dotted lines are mountain folds, red dashed lines are valley folds, and solid black lines are cuts. The folded form is shown in Figure 2(b). The combination of origami and kirigami breaks the kinematic constraints imposed on the fold pattern and reduces the strain of the paper in certain regions, achieving decoupled motion between layers. The drawback is that the cutting also introduces extra undesired degrees of freedom, allowing the structure to deform asymmetrically. In addition, unfolding a single layer results in coupled vertical translation and layer twisting, which makes modeling difficult.

2.3 Final Design

To remove the twisting effect, we modified the crease pattern to align all the layers. Figure 3 shows the final model and corresponding fold pattern. The shaded gray faces were glued together to form a cylindrical surface before folding. The resulting model was the desired stack of concentric rings with different radii. Without any cutting, the motion of each layer could be decoupled. We use this model, which we call Reconfigurable Expanding Bistable Origami (REBO), to create reconfigurable axisymmetric surfaces with independently programmable layers.

3 Reconfigurable Expanding Bistable Origami (REBO)

REBO is a layered origami structure that flattens into a circle and forms a cone when fully extended. Individual layers are circumferentially constrained but can expand or contract in height to change the structure's profile. REBO is constructed from a single 2-D sheet of paper through a sequence of pleats (ref. Figure 3). Placing the pleats at angles allows each row to fold approximately into a circle.

3.1 Design Parameterization

The shape of the folded structure can be controlled through the fold pattern geometry. REBO's profile is a zigzag shape with alternating segments of increasing and decreasing radii. We call one layer of REBO a pair of adjacent segments as shown in Figure 4(b). Let i denote the layer number, with $i = 1$ indicating the top layer, and i increasing towards the bottom layer L. Each layer consists of 2 rows of n identical rectangular units, which we identify as the top and bottom rows.

Figure 4(a) shows example units from two layers. Each unit is a pleated rectangle with the middle crease at an angle of α from horizontal. When these units are used in series, they form an arc, with each unit contributing a rotation angle of

$$\theta = 180° - 2\alpha$$

Figure 4(c) shows a bottom view of the assembled fold pattern with one unit highlighted in green with the corresponding α and θ indicated.

When forming a closed circle, the number of units can be found as

$$n \leq \frac{360°}{\theta}$$

When n is equal to $360°/\theta$, the formed ring should be completely flat. However, when n is smaller than $360°/\theta$, the pattern folds into a conical frustum with a slope angle β. In this case, each layer can be snapped into an extended state, with the top

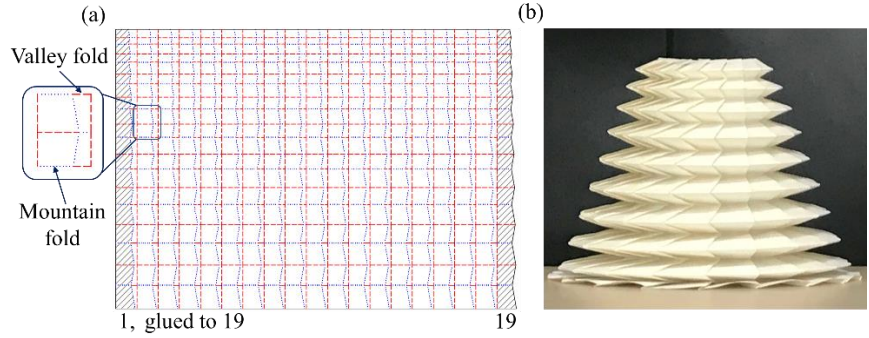

Figure 3: *REBO (a) crease pattern; dotted lines: mountain fold; dashed lines: valley fold; shaded region are units glued together; (b) the folded model.*

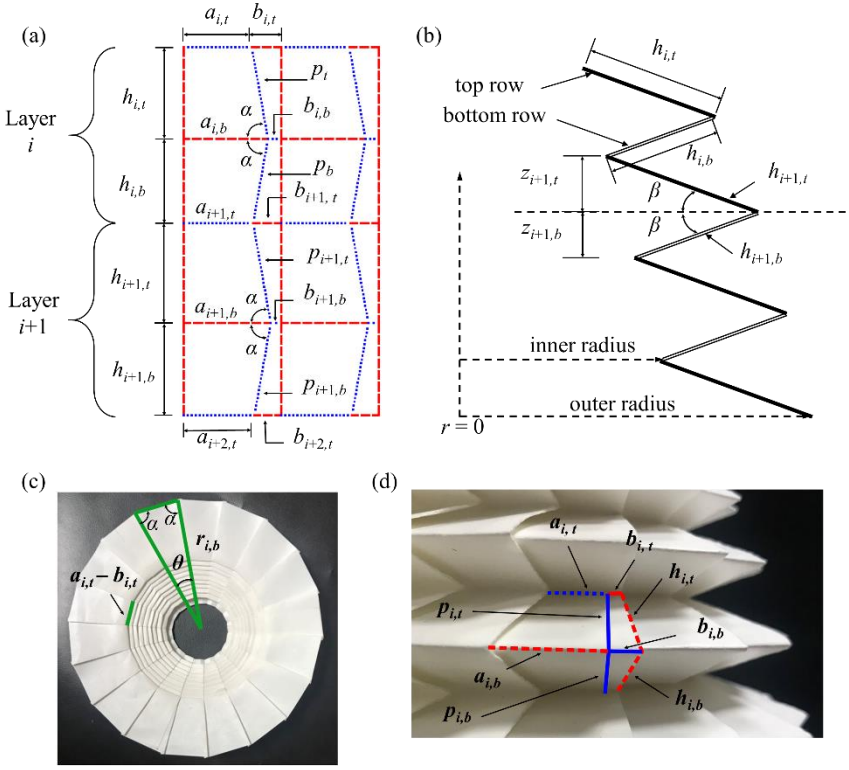

Figure 4: *Geometry of REBO. (a) variables defined on two arbitrary layers of one unit of the crease pattern, dotted lines: mountain fold; dashed lines: valley fold; (b) schematic diagram of the cross-section of the right half of the model consisted of three and a half layers with single lines representing top rows and double lines representing bottom rows. Some other variables are also shown; (c) some variables defined on the model looking from the bottom; (d) 2-D to 3-D crease mapping.* $b_{i,t}$, $b_{i,b}$, $p_{i,t}$ *and* $p_{i,b}$ *cannot be seen from the 3-D model. The solid lines indicate their locations.*

and bottom rows sloped in opposite directions, or into a flattened state, with the top row stacked inside the bottom row. The difference between 360° and $n\theta$, defined as the angular defect ϕ, controls the stability of the layer. The higher the angular defect, the greater the load that must be applied to change the layer's state. Given the angular defect ϕ and the flattened heights $h_{i,t}$ and $h_{i,b}$ of the units in the fold pattern, the slope angle β, the folded height of each top row $z_{i,t}$, and the folded height of each bottom row $z_{i,b}$, shown schematically in Figure 4(b), can be calculated as

$$\beta = \cos^{-1}\left(1 - \frac{\phi}{360°}\right)$$

$$z_{i,t} = h_{i,t}\sin\beta$$

$$z_{i,b} = h_{i,b}\sin\beta$$

Then the extended height of a layer is

$$\Delta z_i = z_{i,t} + z_{i,b}$$

We consider the flattened height of a layer to be four times the thickness t of the paper.

The location of the middle crease inside the unit affects the radius of the layer. We parameterize the location of this crease using the lengths a_i and b_i as indicated on the fold pattern. Parameters a_i and b_i can vary from layer to layer, while the sum of a_i and b_i should be constant. When folded, the creases of length $b_{i,t}$ and $b_{i,b}$ fold onto those with length $a_{i,t}$ and $a_{i,b}$ respectively. Figure 4(d) shows this overlap in REBO's extended form. The lengths $b_{i,t}$ and $b_{i,b}$ cannot be seen from the outside of the 3-D model. The solid lines in Figure 4(d) indicate their locations.

The inner radius $r_{i,t}$ and outer radius $r_{i,b}$ of a layer are then given by

$$r_{i,t} = \frac{1}{2}(a_{i,t} - b_{i,t})\sec\alpha\cos\beta$$

$$r_{i,b} = \frac{1}{2}(a_{i,b} - b_{i,b})\sec\alpha\cos\beta$$

It is important to notice that the condition $a_i > b_i \geq 0$ should always be satisfied; otherwise, the layer cannot be constructed.

The heights of the units $h_{i,t}$ and $h_{i,b}$ also affect the change in radius between layers. For the difference between layers i and i-1, we define two values $\Delta h_{i,t}$ and $\Delta h_{i,b}$ to be

$$\Delta h_{i,t} = h_{i,t} - h_{i-1,t}$$

$$\Delta h_{i,b} = h_{i,b} - h_{i-1,b}$$

The increase in a_i or the decrease in b_i of the bottom row is

$$\Delta a_{i,b} = (h_{i,t} - h_{i-1,b})\cot\alpha$$

Similarly, the increase in a_i or the decrease in b_i of the top row is

$$\Delta a_{i,t} = (h_{i-1,t} - h_{i-1,b})\cot\alpha$$

The increase in radius of each ring is then

$$\Delta r_{i,t} = \Delta a_{i,t} \sec\alpha \cos\beta$$

$$\Delta r_{i,b} = \Delta a_{i,b} \sec\alpha \ \cos\beta$$

In general, $\Delta h_{i,t}$ and $\Delta h_{i,b}$ can vary layer by layer and can be chosen based on the desired resolution of the model. We chose both values to be constant so that the radius changes linearly in our model.

4 Reconfiguration Strategy

In order to approximate a desired surface using this model, individual layers can be selectively extended or flattened. We use a procedure similar to Bresenham's algorithm for discretizing lines [Bresenham 65] to decide which layers should be extended and which layers should remain flat. The procedure is shown in Algorithm 1 and demonstrated in Figure 5.

Given a target height profile z_{tar}, the states of each layer of REBO are determined starting from the bottom layer. For each layer, the extended height of the layer (increase by Δz_i) and the flattened height of the layer (increase by $4t$) are compared to the difference between the target profile and the current height of the previous layer (lines 3-4). In Figure 5, the target profile is represented by the black dotted line, and the flattened and extended heights are shown as circles and squares, respectively. If the extended height is closer in height to the target curve, the layer

Input: Target profile $z_{tar}(r)$, REBO geometry
Output: States of each layer i

1 $z_{L+1} = 0$; // ground height
2 **for** $i = L, L-1, \dots 1$
    // compute difference between target and current height
3 $diff_b = z_{tar}(r_{i,out}) - z_{i+1} - 4t$;
4 $diff_t = z_{tar}(r_{i,out}) - z_{i+1} - \Delta z_i$;

    // Extend or flatten layer to minimize error in z
5 **if** $|diff_t| < |diff_b|$
6 Extend layer *i*;
7 $z_i = z_{i+1} + \Delta z_i$;
8 **else**
9 Flatten layer *i*;
10 $z_i = z_{i+1} + 4t$;
11 **end if**
12 **end for**

Algorithm 1: *Curve approximation using REBO*

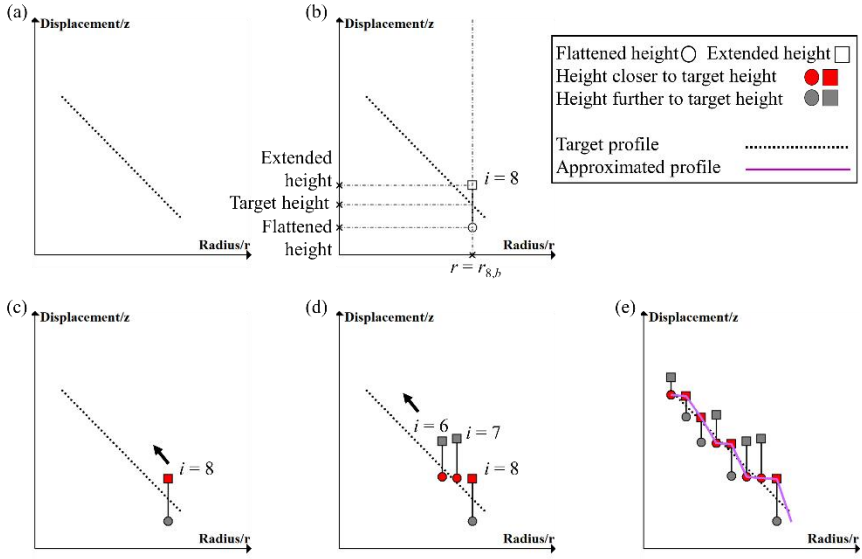

Figure 5: *Steps for curve approximation using REBO. (a) Target profile (black dotted line). (b) Starting from the bottom layer, compare the flattened height (○) and extended height (□) of the layer with the target profile. (c) The state that is closer in height to the target layer is chosen (red), the other one is grayed out. (d) Decisions made for next few higher layers. (e) After the states for all the layers are decided, a magenta solid line representing the approximated surface is found by connecting all the red points.*

will be extended (lines 5-7); if the distance to the flatted height is closer, the layer will not be extended (lines 8-10). For example, in Figure 5(b), the extended height is closer to the target profile, so the layer is extended. This decision is made for each layer to build up the surface (Figures 5(c)-(e)). A magenta dashed line in Figure 5(e) shows the approximated surface by connecting all the red points.

5 Results

We constructed a REBO folded structure from a 63.85[cm] × 44.32[cm] sheet of 0.10[mm] thick Durilla waterproof paper. The folded REBO has a maximum outer radius of 7.62[cm] and a minimum outer radius of 3.26[cm]; it consists of 9 complete layers and a half layer with one additional top row at the base. The radius change between each pair of consecutive layers is 0.55[cm]. Manual reconfiguration is made possible through a small angular defect ϕ of 11.88°, resulting in a slope angle β of 14.76°. The prototype transforms into a cone 11.30[cm] tall when all layers are fully extended.

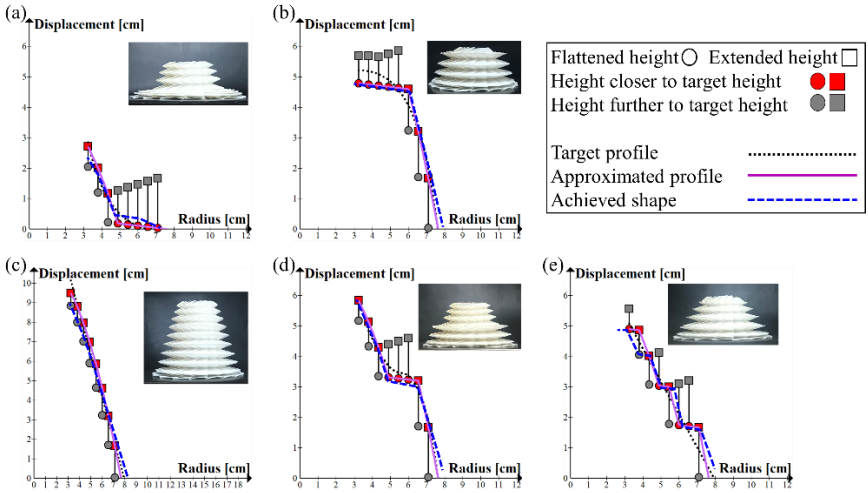

Figure 6: *Selectively extended models and the corresponding profiles. Target profiles are indicated with dotted lines, and computed approximate profiles are indicated with solid lines. The circles and squares show the flattened and extended heights used in the approximation algorithm, with the red fill indicating the chosen state. Dashed lines indicate the experimentally achieved shape. (a) negative Gaussian curvature; (b) positive Gaussian curvature; (c) zero Gaussian curvature with the maximum achievable slope; (d) combination of positive and negative Gaussian curvatures; (e) zero Gaussian curvature with half of the maximum achievable slope.*

We used this structure to approximate shapes with (a) negative Gaussian curvature, (b) positive Gaussian curvature, (c) zero Gaussian curvature, and (d) a combination by manually reconfiguring the REBO according to Algorithm 1. Figure 6 shows the results. The z position of the outer radius of layer 9 was set to zero, and the predicted flattened and extended heights of each layer were computed using the equations in Section 3. The experimentally achieved shapes are shown in dashed lines for comparison. The insets show images of the physical models.

The REBO structure reconfigures reliably and maintains its shape as desired. In all cases, the experimentally achieved shapes are well-matched with the theoretically approximated profiles. Minor errors between the actual and computed approximate profile came from nonuniform extension in the layers, resulting in some tilting between layers, or small differences in predicted and experimental layer height due to the paper weight.

To further test the applicability of the algorithm, we did the same experiment with another zero Gaussian curvature shape shown in Figure 6(e), which has half of the slope of the one in Figure 6(c). Unlike the previous four, where multiple consecutive layers are taking the same state, consecutive layers are taking different

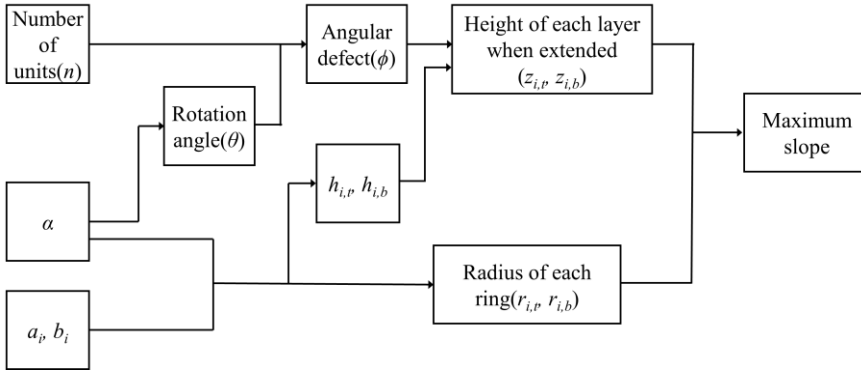

Figure 7: *Effect of fold pattern parameters on folded state of REBO.*

states in Figure 6(e), oscillating around the target profile. The experiment gave the result as expected and further justifies the validity of the approximation algorithm.

6 Discussion

We have designed and demonstrated a reconfigurable origami structure REBO, which consists of a stack of concentric rings with different radii. Each ring can be individually extended or flattened, allowing us to control the surface to produce arbitrary 3-D surfaces. We have shown this ability with negative, positive, zero Gaussian curvatures and other composite curvature profiles.

REBO is a parameterized structure that can be modified to achieve particular sizes and resolutions for surface approximation. Figure 7 provides insights on how each variable is related to the others. The size of each ring is controlled by a_i, b_i, and α. If a bigger ring is desired, a_i - b_i should be increased. The resolution of the pattern is affected by controlling the change in radius and the change in height of each layer. These parameters are controlled through the $h_{i,t}$ and $h_{i,b}$ parameters on the pattern. In particular, higher resolution approximations can be achieved by decreasing $h_{i,t}$ and $h_{i,b}$. to decrease the change in height, and by decreasing $\Delta h_{i,t}$ and $\Delta h_{i,b}$ to decrease the change in radius. The ratio between height changes and radii changes between layers produces the maximum slope achievable by the folded structure. More layers can also be added to increase the size of the structure.

Future work includes studying the mechanism of the snap-through behavior for designing actuated models. The snap-through can be explained geometrically using the angular defect which creates an additional constraint around the circumference of each ring and pushes up the whole ring into a cone-shape structure. However, other fold pattern parameters, such as each layer's radius and height will also affect the stability of the layer. To produce a fully actuated, self-reconfigurable model, further investigation into the precise relationship between these geometric parameters and the mechanical properties of the pattern are needed.

Finally, we can use previous work by [Pikul et al. 17], which shows how the radial strain relates to the 3-D shape's slope, to develop faster and more accurate algorithms for shape control. Combining the concept presented here with future design and actuation work will enable reconfigurable sheets to transform into multiple useful shapes, which can have real-world applications in reconfigurable and deployable structures, such as reconfigurable housing, camouflage, robotic locomotion, and human-machine interfaces.

Acknowledgements

Support for this project was provided in part by National Science Foundation Grant No. 1138847. We are also grateful to Deyuan Chen, who assisted with fabrication. This paper has been awarded the 7OSME Gabriella & Paul Rosenbaum Foundation Travel Award.

References

[Benbernou et al. 11] Benbernou, Nadia, Erik Demaine, Martin Demaine, and Aviv Ovadya. “Universal Hinge Patterns for Folding Orthogonal Shapes.” In *Origami 5*, 405–19 (2011). A K Peters/CRC Press.

[Bresenham 65] Bresenham, J. E. “Algorithm for Computer Control of a Digital Plotter.” *IBM Systems Journal* 4:1 (1965), 25–30.

[Dai and Cannella 08] Dai, Jian S, and Ferdinando Cannella. “Stiffness Characteristics of Carton Folds for Packaging.” *Journal of Mechanical Design* 130:2 (2008), 22305.

[Demaine and O’Rourke 08] Demaine, Erik D, and Joseph O’Rourke. *Geometric Folding Algorithms: Linkages, Origami, Polyhedra* (2008). Cambridge, MA: Cambridge UP.

[Demaine and Tachi 17] Demaine, Erik D, and Tomohiro Tachi. “Origamizer: A Practical Algorithm for Folding Any Polyhedron.” In *Symposium on Computational Geometry* (2017).

[Dudte et al. 16] Dudte, Levi H., Etienne Vouga, Tomohiro Tachi, and L. Mahadevan. “Programming Curvature Using Origami Tessellations.” *Nature Materials* 15:5 (2016), 583–88.

[Edmondson et al. 13] Edmondson, Bryce J., Landen A. Bowen, Clayton L. Grames, Spencer P. Magleby, Larry L. Howell, and Terri C. Bateman. “Oriceps: Origami-Inspired Forceps.” In *Volume 1: Development and Characterization of Multifunctional Materials; Modeling, Simulation and Control of Adaptive Systems; Integrated System Design and Implementation*, V001T01A027 (2013). ASME.

[Evans et al. 15] Evans, Thomas A., Robert J. Lang, Spencer P. Magleby, and Larry L. Howell. “Rigidly Foldable Origami Gadgets and Tessellations.” *Royal Society Open Science* 2:9 (2015), 150067.

[Filipov et al. 15] Filipov, Evgueni T., Tomohiro Tachi, and Glaucio H. Paulino. “Origami Tubes Assembled into Stiff, yet Reconfigurable Structures and Metamaterials.”

Proceedings of the National Academy of Sciences 112:40 (2015), 12321–26.

[Hawkes et al. 10] Hawkes, E, Byoungkwon An, Nadia M Benbernou, H Tanaka, Sangbae Kim, Erik D Demaine, Daniela Rus, and Robert J Wood. "Programmable Matter by Folding." *National Academy of Sciences of the United States of America* 107:28 (2010), 12441–45.

[Hoover et al. 08] Hoover, Aaron M, Erik Steltz, and Ronald S Fearing. "RoACH: An Autonomous 2.4g Crawling Hexapod Robot." In *2008 IEEE/RSJ International Conference on Intelligent Robots and Systems*, 26–33 (2008). IEEE.

[Lang 18] Lang, Robert J. "Twists, Tilings, and Tessellations: Mathematical Methods for Geometric Origami." In , 435 (2018). A K Peters/CRC Press.

[Lang et al. 16] Lang, Robert J., Spencer Magleby, and Larry Howell. "Single Degree-of-Freedom Rigidly Foldable Cut Origami Flashers." *Journal of Mechanisms and Robotics* 8:3 (2016), 31005.

[Liu et al. 17] Liu, Bin, Arthur A. Evans, Jesse L. Silverberg, Christian D. Santangelo, Robert J. Lang, Thomas C. Hull, and Itai Cohen. "Sculpting the Vertex: Manipulating the Configuration Space Topography and Topology of Origami Vertices to Design Mechanical Robustness" (2017), arXiv:1706.01687.

[Overvelde et al. 16] Overvelde, Johannes T.B., Twan A. de Jong, Yanina Shevchenko, Sergio A. Becerra, George M. Whitesides, James C. Weaver, Chuck Hoberman, and Katia Bertoldi. "A Three-Dimensional Actuated Origami-Inspired Transformable Metamaterial with Multiple Degrees of Freedom." *Nature Communications* 7 (2016). Nature Publishing Group, 10929.

[Peraza-Hernandez et al. 14] Peraza-Hernandez, Edwin a, Darren J Hartl, Richard J Malak Jr, and Dimitris C Lagoudas. "Origami-Inspired Active Structures: A Synthesis and Review." *Smart Materials and Structures* 23:9 (2014). IOP Publishing, 94001.

[Pikul et al. 17] Pikul, J. H., S Li, H Bai, R T Hanlon, I Cohen, and R F Shepherd. "Stretchable Surfaces with Programmable 3D Texture Morphing for Synthetic Camouflaging Skins." *Science* 358:6360 (2017), 210–14.

[Rus and Sung 18] Rus, Daniela, and Cynthia Sung. "Spotlight on Origami Robots." *Science Robotics* 3:15 (2018), eaat0938.

[Silverberg et al. 15] Silverberg, Jesse L., Jun-Hee Na, Arthur A. Evans, Bin Liu, Thomas C. Hull, Christian D. Santangelo, Robert J. Lang, Ryan C. Hayward, and Itai Cohen. "Corrigendum: Origami Structures with a Critical Transition to Bistability Arising from Hidden Degrees of Freedom." *Nature Materials* 14:5 (2015), 540–540.

[Thrall and Quaglia 14] Thrall, A.P., and C.P. Quaglia. "Accordion Shelters: A Historical Review of Origami-like Deployable Shelters Developed by the US Military." *Engineering Structures* 59:February (2014). Elsevier Ltd, 686–92.

Hang Yuan
Department of Materials Science and Engineering, University of Pennsylvania, Philadelphia, Pennsylvania, USA, e-mail: yuanhang@seas.upenn.edu

James Pikul
Department of Mechanical Engineering and Applied Mechanics, University of Pennsylvania, Philadelphia, Pennsylvania, USA, e-mail: pikul@seas.upenn.edu

Cynthia Sung
Department of Mechanical Engineering and Applied Mechanics, University of Pennsylvania, Philadelphia, Pennsylvania, USA, e-mail: crsung@seas.upenn.edu